scientific reports

Check for updates

OPEN

Forecasting ocean wave-induced seismic noise

Andrea Bertoldi[1]✉, Stéphane Gaffet[2], Marco Prevedelli[3] & David A. Smith[4]

Ocean waves induce the power peak in the seismic ground motion seen everywhere in the world between 0.03 and ~ 1 Hz, defining the seismic noise baseline. The precise generation mechanisms are well understood, and the dependence of seismic noise on sea weather has been precisely quantified using long-term time series. However, this knowledge has never been exploited to *forecast* the seismic noise background. Here we report the prediction of the seismic noise spectrum around 1 Hz at the Low-Noise Underground Laboratory (LSBB) in Rustrel, for up to 16 days in advance, limited by the time span of sea weather forecasts. We first characterize the dependence of the seismic noise at the LSBB on the Mediterranean Sea and Atlantic Ocean weather, using buoy data for 2020–2021. We exploit significant correlation in the 0.15 Hz $< f <$ 2.5 Hz frequency band to make predictions, converting sea weather forecasts into seismic noise forecasts. The expected seismic background noise can be used to optimize the performance and running costs of scientific and industrial activities, by scheduling them during quiet intervals or adopting adaptive data analysis techniques to identify target signals in the predicted noise.

Wind-generated ocean surface waves cause the microseismic peak observed everywhere on Earth[1–5], and recently they were recognized to be the origin of the "hum" signal[6,7]. Seismic noise at a specific location depends on sea weather, among other factors[8–10]. The role of wind waves has been investigated using long-term time series, which revealed seasonality of the microseismic peak and a strong correlation with the ocean swell and wave activity[9]. The result is a remarkable ability to model seismic noise at a place of interest starting from knowledge of the sea weather, considering the propagation and damping mechanisms of the seismic waves generated by ocean waves[9], or relying on a big-data approach to unveil the dependence[11]. The existing relationship provides insight into sea weather starting from microseism observations[12], and has been proposed to reconstruct past wave climate from seismic records[4]. Building on the established dependence of microseismic noise on sea weather, we report 16 day seismic noise spectrum forecasts at a place of interest[13], and show significant agreement with subsequently recorded spectra over a frequency decade around 1 Hz.

The test-bed site for our forecasting protocol is the LSBB in Rustrel[14], near Apt in Vaucluse, France (see Fig. 1). The underground infrastructure, hosting a French strategic nuclear defense launch control system during the Cold War, is now an interdisciplinary laboratory for science and technology, equipped with extensive instrumentation to study and monitor the local karst system, e.g. optical strainmeters, a hydrostatic long baseline tiltmeter, seismometers, superconducting magnetometers and gravimeters, muon chambers for rock densimetry, and cold atom gravimeters. We chose the site for its extremely low noise environment due to its location far from major anthropogenic disturbances, and for its network of continuously running three-axis broadband seismometers[15], in addition to historic seismic records. We use a Streckeisen STS-2 broadband sensor seismometer located 518 m below the surface (station RUSF, location code 01; see section Material and methods).

In our analyses we use the vertical velocity component. We generate acceleration noise spectra every half hour, by Fourier transforming the 1 h long seismic time signals for the interval centered at the nominal time. To simplify the data treatment, we compute the noise spectra between 0.01 and 10 Hz using 20 frequency bins in geometric progression in each frequency decade.

Sea weather is monitored through several moored weather buoys in the Mediterranean Sea and the Atlantic Ocean, whose measurements are made available by the National Oceanic and Atmospheric Administration (NOAA) and other web services (see section Material and methods). Measurement points are provided every 30 or 60 min, depending on the buoy.

[1]LP2N, Laboratoire Photonique, Numérique et Nanosciences, Université de Bordeaux-IOGS-CNRS, Talence, France. [2]LSBB, Laboratoire Souterrain à Bas Bruit, Avignon Université-CNRS, Rustrel, France. [3]Dipartimento di Fisica e Astronomia, Università di Bologna, Bologna, Italy. [4]Laboratoire d'Astrophysique de Bordeaux, Université de Bordeaux-CNRS, Pessac, France. ✉email: andrea.bertoldi@institutoptique.fr

Figure 1. Buoys' locations and LSBB. The site of interest used to validate the forecast protocol, the LSBB, is indicated with a red icon. Yellow thumbtacks with NOAA ID codes show the 6 buoys considered for the seismic noise forecasts. Image generated with Google Earth™ mapping service. Map Data: Image Landsat / Copernicus, Data SIO, NOAA, U.S. Navy, NGA, GEBCO.

The cause and effect relationship between sea weather and inland seismic noise is clear: ocean waves cause varying pressure at the bottom of the sea, which propagates to distant points as seismic waves in the Earth. The seismic waves generated near each buoy take between a few tens of seconds and a few minutes to reach the LSBB, depending on the distance. Given the time granularity of the buoy data, we assume instantaneous dependence. We remove from the datasets the intervals which contain transient signals covering or competing with the targeted effect , namely seismic events and glitches in the seismic records due to human activities. They are typically characterized by much faster variations than ocean wave generated signals, and can thus be easily filtered out. The intervals identified with our algorithm are cross-validated using earthquake databases (see section Material and methods).

We next compute Pearson's correlation ρ between the variables measured at each buoy and the seismic noise in each spectral bin, to pinpoint the most significant dependencies. For this analysis we used data from February 2020 to November 2021; of the 27 available buoys we selected a representative subset of 3 in the Mediterranean Sea (#01305 Marseille - Le Planier; #61001 Nice; #61002 Golfe du Lion) and 3 in the Atlantic Ocean (#03302 Cap Ferret; #62001 Gascogne Ouest Arcachon; #62163 Bretagne), for their proximity to the LSBB site (see Fig. 1). In the present work we did not consider alternative choices for the number of selected buoys; subsequent sections will elucidate how robust forecasts can be achieved despite this stringent selection process. The correlation matrix shown in Fig. 2 shows three distinctive features: (i) the measurements at the Mediterranean buoys exhibit good correlation with the seismic noise between 0.15 Hz (~ 7 s) and 2 Hz, especially the wave height, period and wind force (positive correlation) and the water and air temperature (negative correlation); (ii) the correlation with the Atlantic buoys is generally less pronounced, but more extended at low frequency and significant down to 0.06 Hz (~ 17 s); (iii) the correlation dips at 0.09 Hz (~ 11 s), due to the reduced seismic noise between the two main natural microseism peaks at ~ 0.07 Hz (~ 14 s) and ~ 0.15 Hz (~ 7 s). As examples, ρ reaches a maximum of 0.9 for the wave heights of buoys #01305 and #61002 around 1 Hz, and 0.3 for that of buoy #62163 at 0.08 Hz (~ 12 s); negative ρ reaches −0.53 for the wave temperature of the buoy #03302 at 0.8 Hz.

Notably, evaluating the correlation between sea weather parameters and the seismic noise could benefit from using historical buoys and seismology data taken during the COVID-19 lockdown, as in our case, leveraging the global reduction in anthropogenic signals within the targeted frequency band[16–18].

Given the correlation plot in Fig. 2, for each buoy we selected the wave height and period, and the wave direction when available, to then run a machine learning algorithm which generates seismic noise spectra starting from sea weather parameters. The other available parameters provide marginal or redundant information, as verified by evaluating their multi-collinearity with the chosen parameters.

We used sea weather forecasts provided by Allosurf[19] for the period from December 5th 2020 to June 27th 2021. Within the available models (see section Material and methods), we used global WAM forecasts, with a resolution of 54 km and extending to 16 days. Interpolating the data from the 4 nearest model mesh points gives the forecasts at the buoy positions.

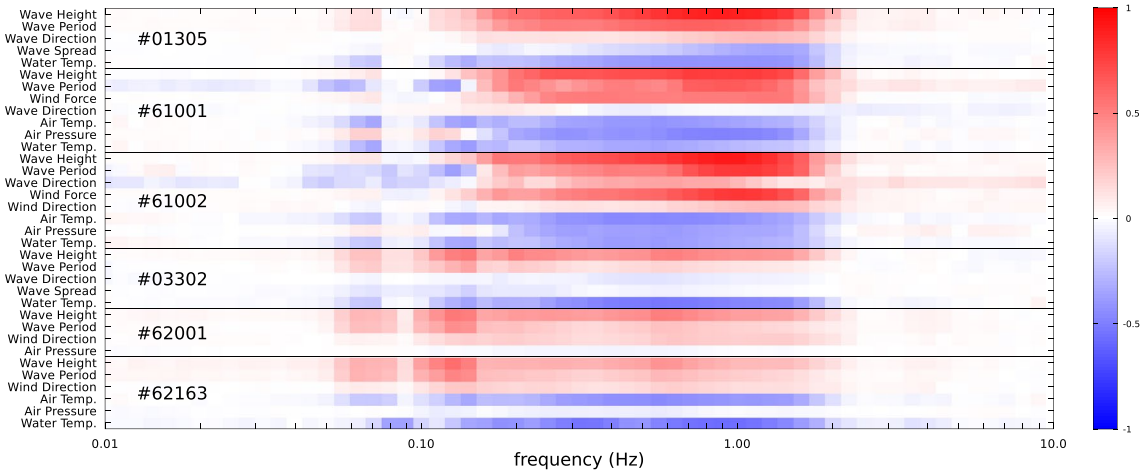

Figure 2. Correlation between seismic noise and ocean weather. Color coded correlation between the spectral components of the seismic noise at LSBB and the sea weather variables measured at the 6 different buoys considered for the seismic noise forecasts.

Next we run the machine learning model, namely a multivariate linear regression between the dependent variables (seismic noise) and the independent ones (sea weather), which assumes a constant uncertainty for the data fitting protocol. Given the wide dynamic range of the data, calm sea weather and seismic conditions contribute only marginally to determining the chi-square. For each day with an available forecast, the model is trained using all data preceding the forecast epoch, and is then applied to the 16 day sea weather forecasts to obtain seismic noise predictions for that period[20]. The predictions are then compared to the seismic spectra measured by the instruments at LSBB, as shown in Fig. 3 in a logarithmic color plot. The period highlighted in the image is characterized by high seismic noise due to the storm Bella[21] at the end of December 2020: the time seismic signal measured at LSBB is shown on the upper graph, and shows the storm peaking on December 28th followed by a minor storm on January 2nd and 3rd. The comparison in the lower panel between the wave heights at the #01305 buoy as predicted on December 24th at 0 am for the next 16 days and that actually measured gives an indication of the sea weather forecast quality. As expected, forecast quality worsens farther into the future, as shown by the increasing difference of the color shades from red on the right of the plot. The forecast validity in the first 8 days is shown by the mainly white and light colours in the frequency intervals characterized by a high correlation in Fig. 2. Remarkably, prediction ability occurs not only in the frequency window related to the double frequency peak ($0.15\ \text{Hz} < f < 2\ \text{Hz}$) but also in the single frequency peak ($0.05\ \text{Hz} < f < 0.08\ \text{Hz}$). Below 0.06 Hz and above 2.5 Hz only noise appears, given the absence of correlation between sea weather and seismic noise.

The spectrum predicted for noon December 28th, i.e. 4.5 days into the future, is shown in the left panel of Fig. 4. The agreement of the forecast with the noise recorded at the LSBB is good in the frequency interval [0.06 Hz: 2.8 Hz], and the uncertainty indicates anew poor predictability around 0.1 Hz. For comparison, the right panel of Fig. 4 reports the forecast for a much quieter period, as shown at the top by the seismic time signal recorded at the site: it consists of the seismic noise spectrum predicted on April 21st for April 29th at 3 pm. Predictability is restricted to the frequency window where the correlation between sea weather and seismic noise is highest, i.e. $0.5\ \text{Hz} < \text{f} < 1.7\ \text{Hz}$, where good agreement is found with the measured seismic noise. The seismic noise spectrum can be especially well predicted for the high noise conditions, when sea weather is the dominant cause of background seismic noise; however, quieter time intervals can also be identified several days in advance because the frequency interval with low prediction uncertainty shrinks around 1 Hz.

After presenting some specific cases, we evaluate prediction accuracy by considering all available forecasts over the ~ 7 month period starting in December 2020, focusing on the 1 Hz frequency bin for the seismic noise. In Fig. 5 we compare the predicted power spectral density of the vertical acceleration (PSD_z) for different time delays into the forecast window with that measured by the seismometer at LSBB. The substantial agreement observed for 1 and 5 day predictions (upper panels in Fig. 5) is replaced by a larger spread of the points relative to a perfect prediction at longer times. Notably, the agreement is strongly enhanced and visible at all times when we focus only on the subset of points for which the ocean weather prediction proved to be precise (red points in Fig. 5); simply, this condition is considered satisfied whenever the measured wave heights at the buoy #01305 are within ±20% of predictions. The seismic prediction obviously depends on the quality of the ocean weather forecasts. The increasingly long and accurate forecasts allowed by the augmenting computational power dedicated to environmental simulations will translate into similarly improved seismic noise forecasts[22].

Finally, we show how ocean-induced seismic noise forecasts could be integrated into planning for scientific or industrial activities requiring low environmental noise.

For a hypothetical measurement campaign, our forecast protocol would provide a go/no-go condition to proceed or not with the planned activity. We consider an experiment which requires at least 12 h with seismic noise at 1 Hz below a given threshold. This activity might require running expensive equipment, and maybe travel for personnel, organized over a one-week measurement campaign.

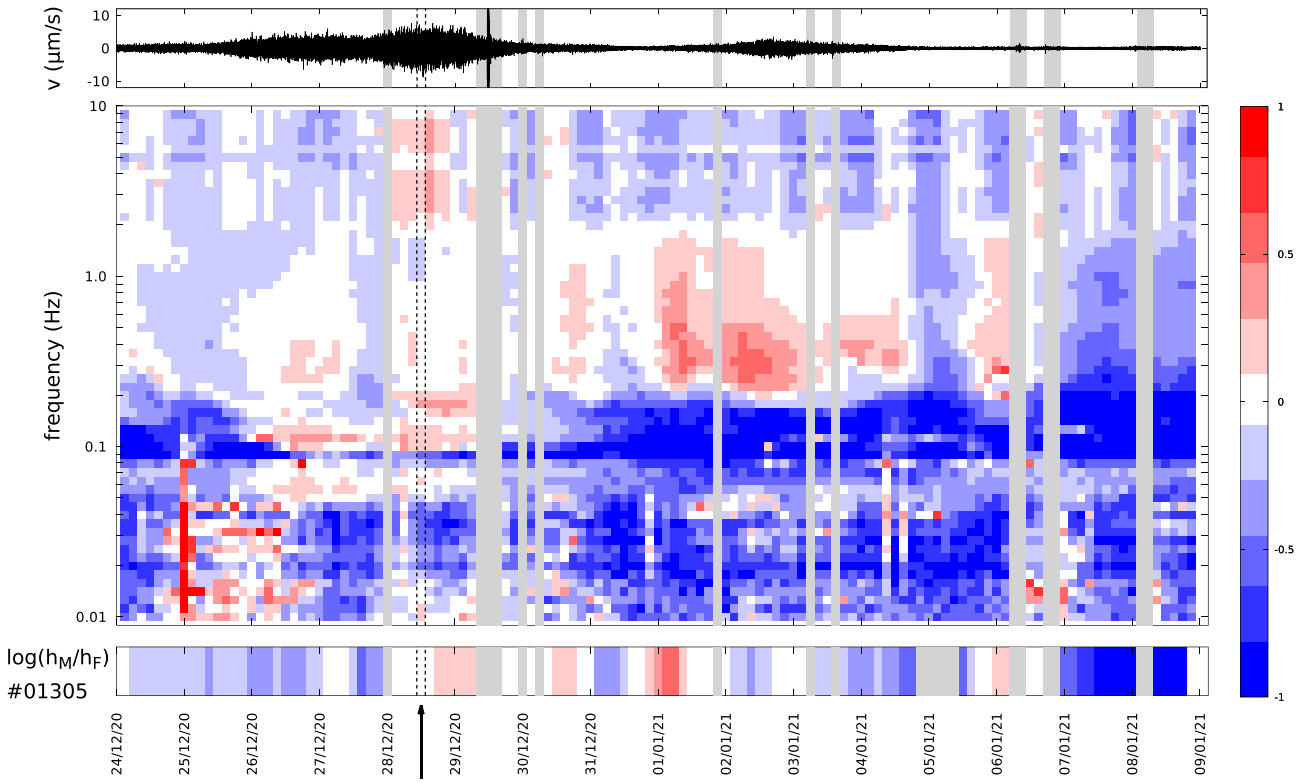

Figure 3. Example of a 16 day long seismic noise forecast. Middle: Logarithm of the ratio between the measured and the predicted seismic noise spectral density in a color plot; white represents a perfect prediction. Bottom: Logarithm of the ratio between the measured and the predicted wave height at the #01305 buoy near Marseilles, indicating the reliability of the weather forecast. Top: Seismic trace of the instantaneous vertical velocity measured at LSBB during the 16 days of the forecast. The forecast centered at noon December 28th, i.e. during the high noise caused by the storm Bella and used in Fig. 4-left, is highlighted by the vertical dashed lines and the arrow. The grey vertical bars indicate time intervals filtered out because of earthquakes, some of which are visible on the upper trace, or data gaps, as for the buoy between January 4th and 5th.

A planned measurement week could be confirmed or canceled based on what our protocol forecasts a few days in advance, to allow preparation time. For example, we could require Thursday's forecast to predict at least one low-noise interval between the following Monday morning and Friday evening. The accuracy of the go/no-go indication in this scenario is always better than 60% over the whole PSD_z range (see Fig. 6, solid black line). When the indication is wrong, in most cases it is a false negative, that is a lost opportunity to exploit a suitable measurement window but without wasting resources (red line). Only rarely were bad noise conditions encountered when good ones had been predicted (blue curve). The protocol can be adapted to specific requirements, and straightforwardly improved to increase its performance. It provides a significant edge over the random choice of a week for a measurement campaign, specifically for a seismic noise threshold $< 5 \times 10^{-15}$ $m^2s^{-4}Hz^{-1}$, given the measured occurrence of the required conditions (grey curve).

The protocol would benefit from incorporating high temporal and spatial resolution ocean data obtained with satellite monitoring[23–25], and by considering also the longitudinal and rotational seismic noise components. Additionally, employing more sophisticated data modelling protocols, such as deep learning techniques, could enhance its predictive capabilities. This would enable forecasting of more detailed noise features, like its polarization, and capturing less evident cause-effect dependencies.

To forecast ocean wave-induced background seismic noise at a specific location, the fundamental requirements include access to data collected by buoys in nearby seas and oceans, as well as the availability of an on-site seismometer. Data from intervals covering typical environmental conditions are used to train the model, ensuring efficient operation.

Sea weather forecasts can be converted into seismic background forecasts over a frequency decade around 1 Hz, with deep potential implications both in fundamental research and applied sciences. The protocol can identify time intervals with low seismic noise several days in advance, with the forecast precision increasing as the time delay shortens. Continuous data collection experiments, like gravitational wave detectors or high-energy particle accelerators, could take advantage of knowing the forthcoming seismic background conditions by implementing adaptive algorithms in their data analysis or thresholding. This advantage is evident for experiments sensitive in the frequency range covered by the seismic noise forecast, as for example in atom interferometers[26–29]. Otherwise, prior knowledge of environmental conditions can be exploited to mitigate the impact of frequency transfer mechanisms, as for example upconversion noise[30,31].

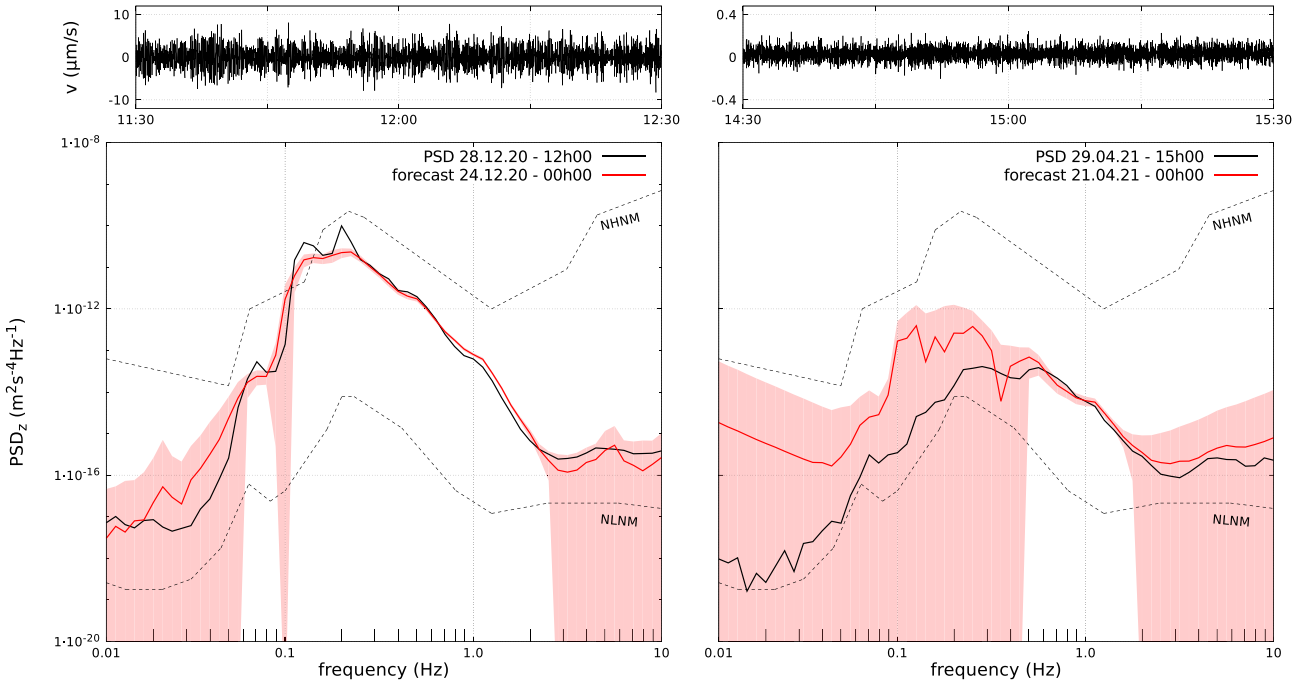

Figure 4. Comparison of forecasted and measured seismic noise spectra. Left: Forecast (red solid line) calculated on 24/12/2020 at 0 am for the seismic spectrum at LSBB (black solid line) on 28/12/2020 at 12 am; these spectra correspond to the data highlighted with dashed lines and arrow in Fig. 3. Right: Forecast calculated on 21/04/2021 at 0 am for the seismic spectrum at LSBB on 29/04/2021 at 3 pm. The pink shaded areas show the forecast one sigma confidence interval; the "new high-noise model" (NHNM) and "new low-noise model" (NLNM) defined by Peterson[3] are reported with dotted lines for reference. The upper panels show 1 h recordings of the vertical velocity at LSBB centered on the nominal time of the forecasts, used to obtain the seismic spectra ; the vertical scale on the right differs by a factor 25.

Material and methods

Seismic noise data at LSBB

For the seismic data at LSBB we use the broadband and three-axial Streckeisen STS-2 seismometer[32] at station RUSF[33], location code 01, the deepest one in the 3D seismic network installed on site, 518 m underground. The access to the continuous seismic processed measurements is provided by the "French seismological and geodetic network" (Résif) webservice[34]. The seismic data are downloaded monthly using a web harvesting robot, which calculates the vertical acceleration spectrum at every half hour and averaging over an hour time interval from the available continuous velocity records. The sampling frequency for the seismic signal is 250 Hz, hence the spectra are binned to reduce the required computation resource for the later steps: the frequency interval between 0.01 and 10 Hz is divided in 60 bins, by adopting a geometric progression (the boundary frequencies are defined by the multiplication factor $\sqrt[20]{10}$).

The time intervals characterized by the presence of earthquakes and other glitches are removed from the datasets, because they mask the targeted dependence between sea weather parameters and the inland seismic background noise. To identify these intervals we look for substantial sudden changes of the seismic noise power spectral density; we set the time integral parameters and the threshold for the variation so as to have a good agreement between the identified intervals and the earthquakes listed in the seismic databases. To this scope we used the NOAA world earthquake database[35] and the IRIS one[36], both mirrored at LSBB[37].

Sea weather data

Sea weather data are continuously retrieved since February 2020 by periodically downloading the information recorded by moored buoys in the sea and oceanic water basins nearby the site of interest, and available for example via the National Data Buoy Center of the NOAA[38], via the Data Buoy Cooperation Panel from the World Meteorological Organization (WMO) and Intergovernmental Oceanographic Commission (IOC) of UNESCO[39], and more specifically for France via the Allosurf website[19]. We refer to the buoys using their WMO station ID code. For the specific case we considered for the validation, targeting the LSBB in Rustrel (France) as site of interest, we downloaded data from 11 buoys in the Atlantic Ocean (#06402 Anglet; #06403 Saint-Jean-de-Luz; #03302 Cap Ferret; #01704 Oleron large; #08504 Ile d'Yeu Nord; #05602 Belle-Ile; #04403 Plateau du Four; #02911 Les Pierres Noires; #62001 Gascogne Ouest Arcachon; #62163 Bretagne; #62029 K1 Atlantique), 5 buoys in the English Channel ((#02204 Brehat - Iles-de-Brehat; #05008 Cherbourg (exterieur); #07607 Paluel; #62305 Manche Greenwich; #62103 Channel Lightship), 2 buoys in the North/Norwegian Sea (#62146 Lomond AWS; #63115 Magnus AWS), and 9 buoys in the Mediterranean Sea (#61001 Nice; #61002 Golfe du Lion; #98000

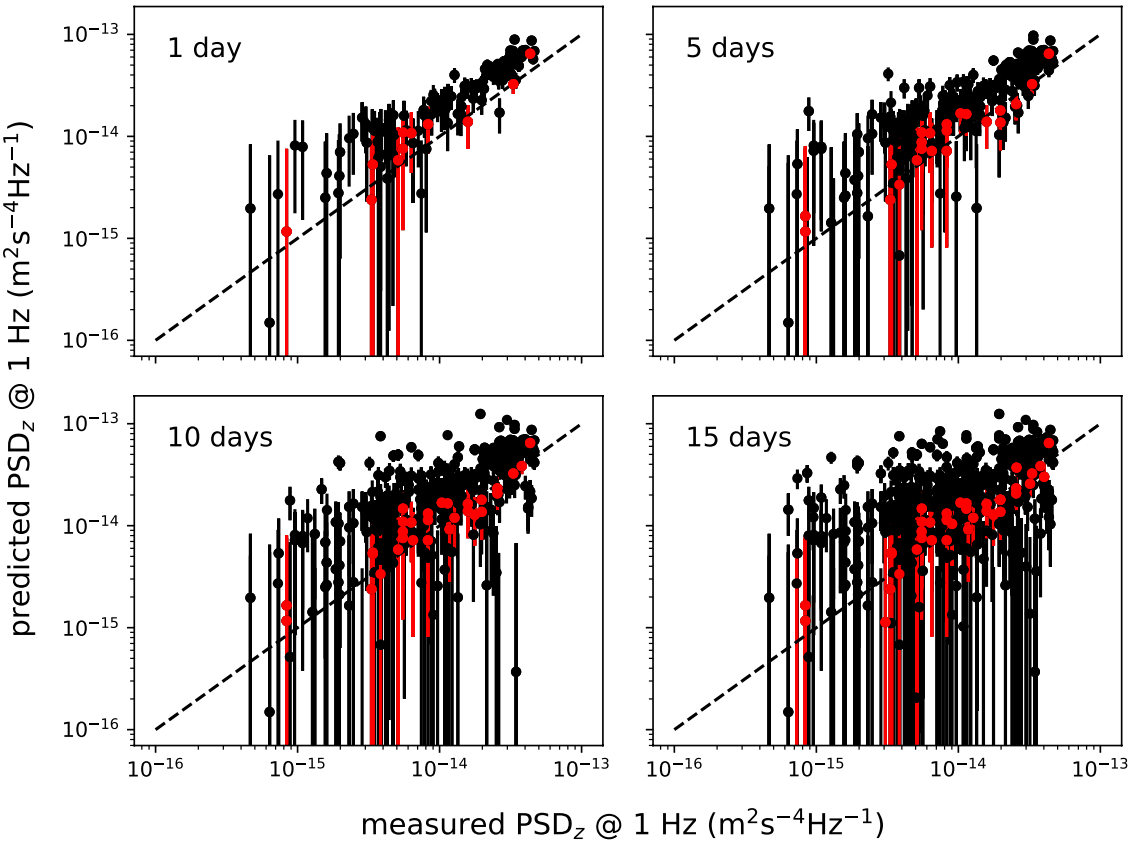

Figure 5. Comparison of forecasted and measured seismic noise at 1 Hz. Predicted versus measured vertical component of the PSD at 1 Hz, for different times into the forecast: 1 day (upper left), 5 days (upper right), 10 days (lower left), and 15 days (lower right). Vertical error bars give the standard error provided by the machine learning model. The points for all available forecasts are in black. Red points show forecasts for which the predicted wave height at buoy #01305 is within ±20% of the measured height. Perfect predictions would lie on the dashed lines.

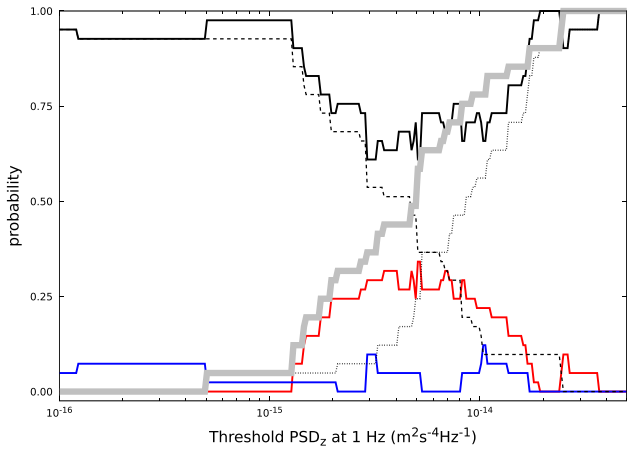

Figure 6. Performance of the go/no-go prediction. Probability of predictions of having a 12 h window with seismic noise background below a given threshold at 1 Hz, made on Thursday for the following week. The different curves represent: success rate (black solid curve), resulting from the sum of the correct go (black dotted line) and no go (black dashed line) predictions; wrong no go prediction (red solid line); wrong go prediction (blue solid line). The measured occurrence of the required conditions is reported with a gray line, which results as the sum of the red curve and the black dotted one. We performed the analysis on 22 weeks of ocean weather forecasts, considering separately forecasts produced at 0 am and 12 am when available for a total of 41 predictions.

Monaco; #08302 Porquerolles; #03001 Espiguette; #03404 Sete; #01101 Leucate; #01305 Marseille - Le Planier; #06601 Banyuls). An interactive view of the buoys position can be seen at[40].

For each buoy several quantities are measured and made available typically every 1 h or 30 min: average and maximal wave height, average and maximal wave period, wave direction and spread, temperature of the water, wind force and direction, air temperature and pressure. Not all the quantities are available for every buoy and at all times. The data are downloaded with a web-scraping script automatically executed twice a day and recovering the last measurement points, which are added to the local data set.

Sea weather forecasts

The Allosurf site[19] provides forecasts maps and the relative raw data for several sea weather parameters (height, period, and direction for the primary and secondary swell, wind speed and direction), based on different kinds of meteorological models. We used the WAM prediction model[41]. Specifically:

- The WAM wave model forecast for the West Mediterranean sea, using a 5 km mesh, with a forecast depth of 96 h;
- The WAM wave model forecast for the Bay of Biscay, using a 1 km mesh, with a forecast depth of 96 h;
- The global forecast WAM wave model, with a resolution of 54 km (or 5°), and a forecast depth of 16 days.

all for the period starting December 5th 2020 and ending June 27th 2021.

Data availability

The main datasets used to produce the results of this study are available from the companion repository[42]: https://doi.org/10.5281/zenodo.7728524.

Received: 20 March 2024; Accepted: 29 August 2024
Published online: 09 September 2024

References

1. Wiechert, E. Verhandlung der Zweiten Internationalen Seismologischen Konferenz. *Beitr. Geophys.* **2**, 41–43 (1904).
2. Longuet-Higgins, M. S. A theory of the origin of microseisms. *Philos. Trans. R. Soc. A* **243**, 1–35. https://doi.org/10.1098/rsta.1950.0012 (1950).
3. Peterson, J. R. Observations and modeling of seismic background noise. *Open-File Report 93-322* (1993). https://doi.org/10.3133/ofr93322.
4. Ardhuin, F., Balanche, A., Stutzmann, E. & Obrebski, M. From seismic noise to ocean wave parameters: general methods and validation. *J. Geophys. Res.* **117**, C05002. https://doi.org/10.1029/2011jc007449 (2012).
5. Nishida, K. Ambient seismic wave field. *Proc. Jpn. Acad. Ser. B, Phys. Biol. Sci.* **93**, 423–448. https://doi.org/10.2183/pjab.93.026 (2017).
6. Webb, S. C. The Earth's hum: the excitation of Earth normal modes by ocean waves. *Geophys. J. Int.* **174**, 542–566. https://doi.org/10.1111/j.1365-246x.2008.03801.x (2008).
7. Ardhuin, F., Gualtieri, L. & Stutzmann, E. How ocean waves rock the Earth: two mechanisms explain microseisms with periods 3 to 300 s. *Geophys. Res. Lett.* **42**, 765–772. https://doi.org/10.1002/2014gl062782 (2015).
8. Wilcock, W. S. D., Webb, S. C. & Bjarnason, I. T. The effect of local wind on seismic noise near 1 Hz at the MELT site and in Iceland. *Bull. Seismol. Soc. Am.* **89**, 1543–1557. https://doi.org/10.1785/bssa0890061543 (1999).
9. Ardhuin, F., Stutzmann, E., Schimmel, M. & Mangeney, A. Ocean wave sources of seismic noise. *J. Geophys. Res.* **116**, C09004. https://doi.org/10.1029/2011jc006952 (2011).
10. Hillers, G. *et al.* Global oceanic microseism sources as seen by seismic arrays and predicted by wave action models. *Geochem. Geophys. Geosyst.* **13**, Q01021. https://doi.org/10.1029/2011gc003875 (2012).
11. Moschella, S. *et al.* Insights into microseism sources by array and machine learning techniques: Ionian and Tyrrhenian Sea case of study. *Front. Earth Sci.* **8**, 1–18. https://doi.org/10.3389/feart.2020.00114 (2020).
12. Bernard, P. L'étude de la houle et de sa prévision par les microséismes. In *Les énergies de la mer. Compte rendu des quatrièmes journées de l'hydraulique, Paris, June 13rd, 14th and 15th 1956. Tome 1, 1957*, Journées de l'hydraulique (1957).
13. Bertoldi, A. & Gaffet, S. Prediction Method of Wave-Induced Background Seismic Noise (2020). EU Patent filing N. EP21305390.
14. Laboratoire Souterrain à Bas Bruit: https://www.lsbb.eu. Accessed 22 July 2024.
15. Gaffet, S. *et al.* A 3d broadband seismic array at LSBB. *IRIS Data Serv. Newsl.* **11**, 3 (2009).
16. Lecocq, T. *et al.* Global quieting of high-frequency seismic noise due to COVID-19 pandemic lockdown measures. *Science* **369**, 1338–1343. https://doi.org/10.1126/science.abd2438 (2020).
17. Poli, P., Boaga, J., Molinari, I., Cascone, V. & Boschi, L. The. Coronavirus lockdown and seismic monitoring of anthropic activities in Northern Italy. *Sci. Rep.* https://doi.org/10.1038/s41598-020-66368-0 (2020).
18. Yabe, S., Imanishi, K. & Nishida, K. Two-step seismic noise reduction caused by COVID-19 induced reduction in social activity in metropolitan Tokyo, Japan. *Earth Planets Sp.* https://doi.org/10.1186/s40623-020-01298-9 (2020).
19. AlloSurf website: https://www.allosurf.net. Accessed 22 July 2024.
20. We also repeated the training using all the available data until Nov 2021, except the 16 days of the forecast, with similar results.
21. Storm Bella: https://en.wikipedia.org/wiki/2020%E2%80%9321_European_windstorm_season#Storm_Bella (2020). Accessed 22 July 2024.
22. Bauer, P., Thorpe, A. & Brunet, G. The quiet revolution of numerical weather prediction. *Nature* **525**, 47–55. https://doi.org/10.1038/nature14956 (2015).
23. Yurovskaya, M., Kudryavtsev, V., Chapron, B. & Collard, F. Ocean surface current retrieval from space: the sentinel-2 multispectral capabilities. *Remote Sens. Environ.* **234**, 111468. https://doi.org/10.1016/j.rse.2019.111468 (2019).
24. Ichikawa, K., Wang, X.-F. & Tamura, H. Capability of Jason-2 subwaveform retrackers for significant wave height in the calm semi-enclosed Celebes sea. *Remote Sens.* **12**, 3367. https://doi.org/10.3390/rs12203367 (2020).
25. Copernicus MEDSEA wave analysis service: https://marine.copernicus.eu/. Accessed 22 July 2024.
26. Dimopoulos, S., Graham, P. W., Hogan, J. M., Kasevich, M. A. & Rajendran, S. Atomic gravitational wave interferometric sensor. *Phys. Rev. D* **78**, 122002. https://doi.org/10.1103/physrevd.78.122002 (2008).
27. Chaibi, W. *et al.* Low frequency gravitational wave detection with ground-based atom interferometer arrays. *Phys. Rev. D* **93**, 021101. https://doi.org/10.1103/physrevd.93.021101 (2016).

28. Canuel, B. *et al.* Exploring gravity with the MIGA large scale atom interferometer. *Sci. Rep.* **8**, 14064. https://doi.org/10.1038/s41598-018-32165-z (2018).
29. Abe, M. *et al.* Matter-wave atomic gradiometer interferometric sensor (MAGIS-100). *Quantum Sci. Technol.* **6**, 044003. https://doi.org/10.1088/2058-9565/abf719 (2021).
30. Effler, A. *et al.* Environmental influences on the LIGO gravitational wave detectors during the 6th science run. *Class. Quantum Gravity* **32**, 035017. https://doi.org/10.1088/0264-9381/32/3/035017 (2015).
31. Aasi, J. *et al.* Characterization of the LIGO detectors during their sixth science run. *Class. Quantum Gravity* **32**, 115012. https://doi.org/10.1088/0264-9381/32/11/115012 (2015).
32. STS-2 seismometer: https://streckeisen.swiss/en/products/sts-2/. Accessed 22 July 2024.
33. RUSF seismic station at LSBB via the Résif network: https://seismology.resif.fr/browse-by-station/#/FR/RUSF. Accessed 22 July 2024.
34. RESIF-RLBP French Broad-Band Network, RESIF-RAP Strong Motion Network and Other Seismic Stations in Metropolitan France. https://doi.org/10.15778/RESIF.FR (1995).
35. NOAA earthquake database: https://www.ngdc.noaa.gov/hazard/earthqk.shtml. Accessed 22-July 2024.
36. IRIS earthquake database: http://ds.iris.edu/seismon/eventlist/index.phtml. Accessed 22 July 2024.
37. LSBB mirror: http://193.52.13.52/vibrato/. Accessed 22 July 2024.
38. National Data Buoy Center: https://www.ndbc.noaa.gov/. Accessed 22 July 2024.
39. Data Buoy Cooperation Panel: https://community.wmo.int/en/data-buoy-co-operation-panel. Accessed 22 July 2024.
40. Buoys on the map: https://www.allosurf.net/meteo/live/carte-bouees.html. Accessed 22 July 2024.
41. The Wamdi Group. The WAM model–a third generation ocean wave prediction model. *J. Phys. Oceanogr.* **18**, 1775–1810. https://doi.org/10.1175/1520-0485(1988)018%3c1775:TWMTGO%3e2.0.CO;2 (1988).
42. Bertoldi, A., Gaffet, S., Prevedelli, M. & Smith, D. A. Forecasting ocean wave-induced seismic noise; supporting dataset. *Zenodo* https://doi.org/10.5281/zenodo.7728524 (2023).

Acknowledgements

We thank Axel Darraba from AlloSurf.net for stimulating discussions, Guillaume Maucort for advice on the data treatment. We acknowledge funding from the "Agence Nationale pour la Recherche" (Grant EOSBECMR # ANR-18-CE91-0003-01).

Author contributions

All authors contributed to designing the research. AB and MP analyzed the data. All authors contributed to the interpretation of the data and preparation of the manuscript.

Competing interests

The authors declare no competing interests.

Additional information

Correspondence and requests for materials should be addressed to A.B.

Reprints and permissions information is available at www.nature.com/reprints.

Publisher's note Springer Nature remains neutral with regard to jurisdictional claims in published maps and institutional affiliations.